Reactive Scattering Dynamics on Conically Intersecting Potential Energy Surfaces: The H + H_2 Exchange Reaction†

Susanta Mahapatra,*,‡,§ Horst Köppel,*,§ and Lorenz S. Cederbaum§

School of Chemistry, University of Hyderabad, Hyderabad 500 046, India, and Theoretical Chemistry, University of Heidelberg, Im Neuenheimer Feld 229, D-69120 Heidelberg, Germany

Received: October 16, 2000; In Final Form: December 12, 2000

We investigate the dynamics of a bimolecular reaction on conically intersecting potential energy surfaces. The flux operator method of calculating the state-specific total reaction probability is extended to a coupled-surface problem, both in the diabatic and adiabatic electronic representations. The reaction probabilities are calculated from their expectation values with the aid of a time-dependent wave packet (WP) approach. The initial WP is prepared in an adiabatic electronic state, and it is propagated in a suitable diabatic electronic representation. The initial state-specific and energy-resolved reaction probability is given in analytical forms in both the adiabatic and diabatic picture. The diagonal correction (Born−Huang term) to the uncoupled adiabatic (Born−Oppenheimer) Hamiltonian is discussed. The above formalism is applied to the H + H_2 exchange reaction on its conically intersecting double many-body expansion (DMBE) potential energy surfaces. We report the initial state-selected reaction probabilities for energies extending up to the onset of the three-body dissociation of this system. We find only a minor impact of the conical intersection on the reactive scattering dynamics of H + H_2. A closer inspection of the electronic population reveals a very small fraction of the WP traversing the upper adiabatic sheet during the course of the reaction. The accuracy of the DMBE potential energy surface is assessed by comparing with new ab initio data.

I. Introduction

Conical intersections of electronic potential energy surfaces are a generic feature of polyatomic molecules.[1−6] Such intersections lead to a breakdown of the Born−Oppenheimer approximation and initiate new mechanisms ensuing different nonadiabatic couplings and highly complex nuclear dynamics.[7] The consequences of conical intersection in the spectroscopy of bound molecular systems are well understood (see, for example, refs 2 and 4 and references therein). More recently, their possible implications for molecular scattering systems have also become a major issue. The effect of conical intersections on the state-specific and the state-to-state reactive and nonreactive scattering attributes was demonstrated with an extended two coordinate quasi Jahn−Teller (JT) model.[8] The effect of nonadiabatic couplings has been realized on the dynamics of O + H_2 (HD) insertion and abstraction reactions in a quasiclassical trajectory study.[9,10] Whiteley et al.[11] have performed a quantum scattering study on the coupled electronic states Cl(^{2}P) + HCl reaction using a coupled channel reactive scattering method based on hyperspherical coordinates. The product energy distributions in the photodissociation of triatomic molecules, for example O_3 and H_2S, on their conically intersecting potential energy surfaces have also been studied.[12,13] Quantum scattering calculations using coupled potential energy surfaces are generally cumbersome and difficult to perform.

In the present article we aim to investigate the effects of conical intersections on the reaction probability of a bimolecular collision process. A time-dependent wave packet (WP) method is extended to the ($E \times \epsilon$)-JT conical intersection for this purpose. The initial wave packet is prepared in an adiabatic electronic state, thus reflecting the experimental conditions. To avoid the numerical instabilities arising from the diverging nature of the nonadiabatic couplings in this representation[14] the WP is propagated in a suitable *diabatic* electronic representation.[15] The initial state-specific total reaction probabilities are calculated by representing the flux operator both in the adiabatic as well as in the diabatic electronic representation. This enables us to establish a connection between the results obtained in the two representations. As far as we are aware this is for the first time such an analysis has been performed in a reactive scattering study.

We apply the above formalism to the H + H_2 exchange reaction on its conically intersecting double many-body expansion (DMBE) potential energy surfaces.[16] The prototypical hydrogen exchange reaction

$$H + H_2 \rightarrow H_2 + H \qquad \text{(R1)}$$

is one of the cornerstones in our understanding of the microscopic details of the reactive scattering dynamics. The ground electronic state of H_3 is orbitally degenerate at the D_{3h} symmetry configuration. In 1968 Porter et al.[17] established that the two sheets of its ground electronic potential energy surface (PES) exhibit a conical intersection at the point of degeneracy. They established the resemblance of this system to other ($E \times \epsilon$)-JT active systems.[18] Many improved and high-quality ab initio PESs for the lower adiabatic sheet of its ground electronic manifold appeared in the literature.[16,19,20] However, to date, the DMBE PES[16] is the only PES available for this system which globally represents both the lower and the upper adiabatic sheets of the

† Part of the special issue "Aron Kuppermann Festschrift".

* To whom correspondence should be addressed. E-mail: S.M., smsc@uohyd.ernet.in; H.K., horst@tc.pci.uni-heidelberg.de. Fax: H.K., +49-6221-545221.

‡ University of Hyderabad.

§ University of Heidelberg.

10.1021/jp003784b CCC: $20.00
Published on Web 02/17/2001

ground electronic manifold of H_3 and offers a possibility to study theoretically the nonadiabatic effects associated with the conical intersection on its nuclear dynamics.

The effects of this conical intersection on the reactive scattering dynamics of (R1) and its isotopic variants were studied quantum mechanically for the first time by Kuppermann and co-workers.[21] They performed calculations with the lower adiabatic sheet of the PES incorporating these effects in terms of the geometric phase (GP) change of the wave function when encircling the conical intersection in a closed path, without explicitly considering both sheets of the PES and the nonadiabatic couplings between them. They have shown that the differential cross sections for the $H + D_2(v = 0)$ exchange reaction at a collision energy of 1.29 eV agree well with the experimental results when the GP change is taken into consideration.[22] In a later study Schnieder et al. have reproduced the fully state-resolved measurements of ultrahigh resolution without taking the GP effects into consideration.[23] In view of the fact that the minimum of the seam of the conical intersections in this system occurs at an energy of ~2.74 eV,[16] it is not clear whether any noticeable effects of GP change can be seen on its reactive scattering dynamics much below this energy. Furthermore, the GP effects are intricately dependent on the topology of the PES and any small disturbances in the latter can cause a noticeable change in the differential cross sections. Recently Kendrick has performed very accurate scattering calculations quantum mechanically and found no noticeable GP effects on the dynamics of this reaction.[24]

While the GP effects at an energy much below that of the minimum of the seam of conical intersections on the reactive scattering dynamics of (R1) are a debatable issue, they were shown to have only negligible influence on the transition state resonances of H_3 (originating from the saddle point region of the PES at the collinear arrangements of the three nuclei).[25] Furthermore, coupled surface studies explicitly considering the nonadiabatic couplings also did not reveal any effect on these resonances.[26] Due to the fact that the conical intersections occur at the D_{3h} equilibrium geometry of H_3, the saddle point resonances are not affected by the strong nonadiabatic effects. The direct evidence of the strong nonadiabatic effects emerged from the neutralized ion-beam experiment of Bruckmeier et al.[27] which probed H_3 in the vicinity of the intersection seam of the 1E′ electronic manifold. In later theoretical studies Mahapatra and Köppel[28] have unambiguously established the importance of the nonadiabatic coupling in this simple polyatomic system complementing the experimental results of Bruckmeier et al.[27]

Despite the aforementioned works on this system a study of the reactive scattering dynamics of (R1) employing two interacting electronic states is still missing. In the present work we apply the formalism mentioned above to fill this gap. The reaction probabilities are reported for energies up to the onset of the three-body dissociation of H_3. Our results indicate *no noticeable effects* of the conical intersection on the state-specific dynamics of this system. As a matter of fact, the coupled-state results can essentially be reproduced by an uncoupled surface calculation, especially when including the diagonal (or Born−Huang) correction to the BO Hamiltonian. We find that a very small fraction of the WP traverses the conical intersection during the course of the reaction. These findings extend the recent studies on this system by going to higher energies and incorporating GP effects and the nonadiabatic couplings in a coherent fashion.

The rest of the paper is organized in the following way. In section II we present the theory describing the Hamiltonian and the flux operator and the reaction probability both in the diabatic as well as in the adiabatic electronic representations. The diagonal correction to the BO adiabatic Hamiltonian is also discussed. In section III we give some computational details of the reaction probability. In section IV we present the numerical results obtained on the $H + H_2$ exchange reaction and briefly discuss them. Finally the paper is closed with a succinct summary in section V.

II. Theory

In this section we describe the formalism to calculate the reaction probability on a coupled electronic manifold. The reaction probability is obtained in the usual way from the expectation value of the flux operator on the basis of the energy-normalized time-independent reactive scattering wave function.[29−33] In the following we describe the theory using the $H + H_2$ exchange reaction as a reference. The reactive scattering of $H + H_2$ occurs on the repulsive lower adiabatic sheet of its ground electronic manifold. We prepare the initial wave packet pertinent to the reagents in the asymptotic reactant channel of this sheet (as is the case in all previous studies). To propagate this WP in time we resort to a diabatic electronic representation.[15] The *divergent* nature of the nonadiabatic couplings appearing in the adiabatic electronic representation at the point of degeneracy of the two surfaces is avoided in a diabatic representation.[2] Finally the reaction probability can be calculated in either way by representing the flux operator in the diabatic or in the adiabatic electronic basis.

A. Diabatic Electronic Representation. *1. Hamiltonian.* The diabatic Hamiltonian for the ground (1E′) electronic manifold of the $H + H_2$ system can be written as

$$\begin{aligned} \mathsf{H}^{\mathrm{d}} &= \mathsf{H}^{Nu} + \mathsf{H}^{el} \\ &= T_{\mathrm{N}}\begin{pmatrix} 1 & 0 \\ 0 & 1 \end{pmatrix} + \begin{pmatrix} U_{11} & U_{12} \\ U_{21} & U_{22} \end{pmatrix} \end{aligned} \tag{1}$$

where H^{Nu} and H^{el} are the nuclear and the electronic parts of the Hamiltonian matrix. T_{N} represents the nuclear kinetic energy operator and U_{11} and U_{22} are the energies of the two diabatic electronic states coupled by the potential matrix elements $U_{12} = U_{21}$. T_{N}, in the mass-scaled reactant channel body-fixed Jacobi coordinates (R, r, γ) and for the total angular momentum $J = 0$ is given by[34]

$$\begin{aligned} T_{\mathrm{N}} &= \frac{1}{2\mu}[P_R^{\,2} + P_r^{\,2}] + \frac{\boldsymbol{j}^2}{2I} \\ &= -\frac{\hbar^2}{2\mu}\left[\frac{\partial^2}{\partial R^2} + \frac{\partial^2}{\partial r^2}\right] - \frac{\hbar^2}{2I}\frac{1}{\sin\gamma}\frac{\partial}{\partial\gamma}\left(\sin\gamma\frac{\partial}{\partial\gamma}\right) \end{aligned} \tag{2}$$

Here P_R and P_r are the momentum operators corresponding to the two Jacobi distances R (distance of H from the center-of-mass of H_2) and r (scaled H_2 internuclear distance), respectively. $\boldsymbol{j}$ is the H_2 rotational angular momentum operator associated with the Jacobi angle γ (angle between $\vec{R}$ and $\vec{r}$). The quantity μ, $\mu = m_{\mathrm{H}}/3^{1/2}$ (m_{H} is the mass of the H nuclei), is the three-body uniform (for both channels R and r) reduced mass, and I, $I = \mu R^2 r^2/(R^2 + r^2)$, is the three-body moment of inertia. The body-fixed z axis is defined to be parallel to $\vec{R}$ and H_2 lies in the (x, z) plane.

The elements of the diabatic electronic Hamiltonian matrix in eq 1 are obtained by diabatizing the (diagonal) adiabatic electronic Hamiltonian matrix through the following similarity transformation:

$$\begin{pmatrix} U_{11} & U_{12} \\ U_{21} & U_{22} \end{pmatrix} = \boldsymbol{S}\begin{pmatrix} V_- & 0 \\ 0 & V_+ \end{pmatrix}\boldsymbol{S}^\dagger = \frac{V_+ + V_-}{2}\mathbf{1} + \frac{V_+ - V_-}{2}\begin{pmatrix} -\cos\chi & \sin\chi \\ \sin\chi & \cos\chi \end{pmatrix} \quad (3)$$

with ($\alpha = \chi/2$)

$$\boldsymbol{S} = \begin{pmatrix} \cos\alpha & \sin\alpha \\ -\sin\alpha & \cos\alpha \end{pmatrix} \quad (4)$$

Here **1** is a 2 × 2 unit matrix and ***S*** is the unitary transformation matrix from the adiabatic to the diabatic representation, $\Psi_d = \boldsymbol{S}\Psi^{ad}$; α is the adiabatic−diabatic mixing angle. The quantities V_- and V_+ are the potential energies of the lower and the upper adiabatic sheets of the DMBE PES of H_3,[16] respectively. The angle χ, $\chi = 2\alpha$, is identified with the pseudorotation angle, defined as the direction of the ϵ-type displacement in its two-dimensional vibrational subspace of the D_{3h} point group.[16,35,36] This method of diabatization was tested numerically with a second-order model ($E \times \epsilon$)-JT Hamiltonian by Thiel and Köppel.[36] It was shown that with this scheme of diabatization the singular derivative coupling terms are eliminated and the matrix elements of the residual derivative couplings become vanishingly small.[36] We also applied this scheme successfully in our earlier investigations on the Rydberg emission spectrum of H_3.[28,35] A similar line of work has been followed by Yarkony.[37]

2. Flux Operator and Reaction Probability. The flux operator $\hat{F}$ is defined in terms of a dividing surface Θ which is a function of a suitable coordinate that separates the products from the reactants[38]

$$\hat{F} = \frac{i}{\hbar}[H^{\,d}, \Theta] \quad (5)$$

In the present case an obvious choice for Θ is given by

$$\Theta = h(r - r_d) \quad (6)$$

where h is a heaviside step function which equals unity for positive argument and zero otherwise. r_d is to be chosen far out in the product channel to ensure the asymptotic motion for all $r \geq r_d$. Since Θ depends only on coordinates, the electronic part of $H^{\,d}$ commutes with it; therefore eq 5 becomes

$$\hat{F} = \frac{i}{\hbar}[T_N, \Theta] \quad (7)$$

In a diabatic representation the kinetic energy operator T_N is diagonal (eq 1); therefore, the flux operator possesses the same property in this representation. Its nonzero diagonal elements are given by

$$\hat{f}_{11} = \hat{f}_{22} = \frac{-i\hbar}{2\mu}\left[\frac{\partial}{\partial r}\delta(r - r_d) + \delta(r - r_d)\frac{\partial}{\partial r}\right] \quad (8)$$

The reaction probability is the expectation value of the above flux operator in the basis of the energy normalized time-independent reactive scattering wave function evaluated at $r = r_d$. We write this wave function in the diabatic basis as

$$|\Phi^d(R,r_d,\gamma,E)\rangle = \begin{pmatrix} |\phi_1^d(R,r_d,\gamma,E)\rangle \\ |\phi_2^d(R,r_d,\gamma,E)\rangle \end{pmatrix} \quad (9)$$

where $\phi_1^{\,d}$ and $\phi_2^{\,d}$ correspond to the wave function components on the diabatic states 1 and 2, respectively. For an initial state i (corresponding to a specific vibrational v and rotational j state of the reagent H_2) the energy resolved reaction probability is given by

$$P_i^R(E) = \sum_f |S_{fi}^R|^2 = \langle \Phi^d(R,r_d,\gamma,E)|\hat{F}|\Phi^d(R,r_d,\gamma,E)\rangle \quad (10)$$

where S_{fi}^R is the reactive scattering matrix from an initial state (i) of the reactant to a final state (f) of the product. In terms of the component diabatic wave functions the above equation can be written as

$$P_i^R(E) = \sum_{k=1}^{2}\langle \phi_k^{\,d}(R,r_d,\gamma,E)|\hat{f}_{kk}|\phi_k^{\,d}(R,r_d,\gamma,E)\rangle = \frac{\hbar}{\mu}\sum_{k=1}^{2}\mathrm{Im}\left[\left\langle \phi_k^{\,d}(R,r_d,\gamma,E)\left|\frac{\partial\phi_k^{\,d}(R,r_d,\gamma,E)}{\partial r}\right\rangle\right]_{|r=rd} \quad (11)$$

The quantity in the right-hand side of the above equation is integrated over the entire range of R and γ. The energy normalized time-independent reactive scattering wave function is calculated along the dividing surface at $r = r_d$ as

$$|\phi_k^{\,d}(R,r_d,\gamma,E)\rangle = |\psi_k^{\,d}(R,r_d,\gamma,E)\rangle/\kappa_E \quad (12)$$

The function $|\psi_k^{\,d}(R,r_d,\gamma,E)\rangle$ is obtained by Fourier transforming the time-evolved wave packet $|\psi_k^{\,d}(R,r,\gamma,t)\rangle$ along the dividing surface

$$|\psi_k^{\,d}(R,r_d,\gamma,E)\rangle = \frac{1}{\sqrt{2\pi}}\int_{-\infty}^{+\infty} e^{iEt/\hbar}|\psi_k^{\,d}(R,r,\gamma,t)\rangle\, dt|_{r=rd} \quad (13)$$

The quantity κ_E in eq 12 is the weight of the translational component $F(R)$ (see eq 29) contained in the initial wave packet for a given total energy E

$$\kappa_E = \left(\frac{\mu}{2\pi\hbar k}\right)^{1/2}\int_{-\infty}^{+\infty} F(R)e^{ikR}\, dR \quad (14)$$

where $k = \sqrt{2\mu(E-\epsilon_{vj})/\hbar}$, with ϵ_{vj} being the initial rovibrational energy of the H_2 molecule.

B. Adiabatic Electronic Representation. *1. Hamiltonian.* In the adiabatic electronic representation the electronic part of the Hamiltonian is diagonal and the nonadiabatic coupling elements appear as off-diagonal elements in the nuclear part. The adiabatic Hamiltonian matrix can be obtained from the diabatic one of eq 1 through the following similarity transformation:

$$H^{\,ad} = \boldsymbol{S}^\dagger H^{\,d}\mathbf{S} = T_N\mathbf{1} + \boldsymbol{S}^\dagger[T_N,\boldsymbol{S}] + \begin{pmatrix} V_- & 0 \\ 0 & V_+ \end{pmatrix} \quad (15)$$

where T_N represents the nuclear kinetic energy operator given in eq 2. The nonadiabatic coupling matrix is given by

$$\Lambda = -\boldsymbol{S}^\dagger[T_N,\boldsymbol{S}] \quad (16)$$

The matrix Λ has a diagonal (e.g. Λ^0) and an off-diagonal (e.g. Λ') part; Λ is set to zero in the usual Born−Oppenheimer picture. However, when its diagonal elements are retained, one arrives at the Born−Huang Hamiltonian.[40] Using the diabatic Hamiltonian matrix of eq 1 and the rotation matrix ***S*** of eq 4, after some rigorous algebra the following adiabatic Hamiltonian is obtained:

$$H^{ad} = T_N\begin{pmatrix}1 & 0\\ 0 & 1\end{pmatrix} + \begin{pmatrix}V_- & 0\\ 0 & V_+\end{pmatrix} + \left[\frac{\hbar^2}{2\mu}(\alpha_R'^2 + \alpha_r'^2) + \frac{\hbar^2}{2I}\alpha_\gamma'^2\right]\begin{pmatrix}1 & 0\\ 0 & 1\end{pmatrix} + \left[\frac{\hbar^2}{2\mu}\left(\alpha_R'' + 2\alpha_R'\frac{\partial}{\partial R} + \alpha_r'' + 2\alpha_r'\frac{\partial}{\partial r}\right) + \frac{\hbar^2}{2I}\left(\alpha_\gamma'' + 2\alpha_\gamma'\frac{\partial}{\partial \gamma} + \alpha_\gamma' \cot\gamma\right)\right]\begin{pmatrix}0 & -1\\ 1 & 0\end{pmatrix} \quad (17)$$

where $\alpha_x' = \partial\alpha/\partial x$ and $\alpha_x'' = \partial^2\alpha/\partial x^2$. The third term in the right-hand side of eq 17 corresponds to the Born−Huang term Λ^0.

The adiabatic−diabatic mixing angle α is a "complicated" function of the Jacobi coordinates, and an evaluation of Λ in these coordinates is cumbersome. This can be better accomplished in the ($E \times \epsilon$)-JT coordinates ρ_{JT} and χ. The latter are identified as the radius of the JT displacement and the pseudorotation angle (introduced in section II.A.1), respectively. These coordinates can be expressed in terms of the Cartesian normal coordinates (dimensionless) of the ϵ-type vibration (Q_x and Q_y) of the D_{3h} point group as

$$\rho_{JT}e^{i\chi} = Q_x + iQ_y \quad (18)$$

In these coordinates the BH term is given by[36,41]

$$\Lambda^0(\tilde{\alpha}) = \frac{\omega_\epsilon\hbar}{8}\left[\left(\frac{\partial\tilde{\alpha}}{\partial\rho_{JT}}\right)^2 + \frac{1}{\rho_{JT}^2}\left(\frac{\partial\tilde{\alpha}}{\partial\chi}\right)^2\right] \quad (19)$$

where ω_ϵ is the frequency of the degenerate vibration and $\tilde{\alpha} = 2\alpha$. Within the linear coupling scheme $\tilde{\alpha} = \chi$ (eq 3) and does not depend on ρ_{JT}, and therefore, eq 19 is given by

$$\Lambda^0 = \frac{\omega_\epsilon\hbar}{8\rho_{JT}^2} \quad (20)$$

In terms of the mass-weighted coordinate q_{JT} to be used below, eq 20 reads

$$\Lambda^0 = \frac{\hbar^2}{8m_H q_{JT}^2} \quad (21)$$

We mention that the BH term of interest here is only the term diverging at the conical intersection. Within the general framework of the "adiabatic correction" as analyzed, e.g. by Kutzelnigg in ref 42, this is given by part c of his eq 21.

2. Flux Operator and Reaction Probability. We require an expression for the flux operator in the adiabatic electronic basis to calculate the reaction probability in this basis for the present two-state problem. Since in the definition of the flux operator, Θ, depends only on the reaction coordinate (here r), only the r-dependent part of the nuclear kinetic energy operator is of relevance in eq 7. It can be seen from eq 17 that the nuclear kinetic energy operator is nondiagonal and its r-dependent part is given by

$$T_r^{ad} = \frac{-\hbar^2}{2\mu}\begin{pmatrix}\frac{\partial^2}{\partial r^2} - \alpha_r'^2 & \left(\alpha_r'' + 2\alpha_r'\frac{\partial}{\partial r}\right)\\ -\left(\alpha_r'' + 2\alpha_r'\frac{\partial}{r}\right) & \frac{\partial^2}{\partial r^2} - \alpha_r'^2\end{pmatrix} \quad (22)$$

Since T_r^{ad} is nondiagonal the flux operator will have the same property in the adiabatic electronic basis. On substituting T_r^{ad} in eq 7, one arrives at the same expression as in eq 8 for the diagonal elements ($\hat{f}_{11}$ and $\hat{f}_{22}$) of the flux operator in the adiabatic basis, and its off-diagonal elements are given by

$$\hat{f}_{12} = -\hat{f}_{21} = \frac{-i\hbar\alpha_r'}{\mu}\delta(r - r_d) \quad (23)$$

We define the energy normalized time-independent reactive scattering wave function in the adiabatic electronic basis as

$$|\Phi^{ad}(R,r_d,\gamma,E)\rangle = \begin{pmatrix}|\phi_-^{ad}(R,r_d,\gamma,E)\rangle\\ |\phi_+^{ad}(R,r_d,\gamma,E)\rangle\end{pmatrix} \quad (24)$$

where ϕ_-^{ad} and ϕ_+^{ad} represent the two components of this wave function on V_- and V_+, respectively. The reaction probability in the adiabatic electronic representation is then given by

$$P_i^R(E) = \langle\Phi^{ad}(R,r_d,\gamma,E)|\hat{F}|\Phi^{ad}(R,r_d,\gamma,E)\rangle = \frac{\hbar}{\mu}\left[\mathrm{Im}\left\langle\phi_-^{ad}(R,r_d,\gamma,E)\left|\frac{\partial\phi_-^{ad}(R,r_d,\gamma,E)}{\partial r}\right\rangle + \mathrm{Im}\left\langle\phi_+^{ad}(R,r_d,\gamma,E)\left|\frac{\partial\phi_+^{ad}(R,r_d,\gamma,E)}{\partial r}\right\rangle + \mathrm{Im}\langle\phi_-^{ad}(R,r_d,\gamma,E)|\alpha_r'|\phi_+^{ad}(R,r_d,\gamma,E)\rangle - \mathrm{Im}\langle\phi_+^{ad}(R,r_d,\gamma,E)|\alpha_r'|\phi_-^{ad}(R,r_d,\gamma,E)\rangle\right] \quad (25)$$

The wave functions ϕ_-^{ad} and ϕ_+^{ad} can be obtained in an analogous way as described for ϕ_1^d and ϕ_2^d. Since α_r' is a real quantity, the last two terms of eq 25 are complex conjugate to each other and therefore $P_i^R(E)$ becomes

$$P_i^R(E) = \frac{\hbar}{\mu}\left[\mathrm{Im}\left\langle\phi_-^{ad}(R,r_d,\gamma,E)\left|\frac{\partial\phi_-^{ad}(R,r_d,\gamma,E)}{\partial r}\right\rangle + \mathrm{Im}\left\langle\phi_+^{ad}(R,r_d,\gamma,E)\left|\frac{\phi_+^{ad}(R,r_d,\gamma,E)}{\partial r}\right\rangle + 2\mathrm{Im}\langle\phi_-^{ad}(R,r_d,\gamma,E)|\alpha_r'|\phi_+^{ad}(R,r_d,\gamma,E)\rangle\right] \quad (26)$$

Contrary to the analogous expression (eq 11) in the diabatic basis, the result (eq 26) contains also off-diagonal electronic contributions. These are expected to play an important role when both channels, corresponding to V_- and V_+ are open. If only V_- is open then only the first of the three terms on the right-hand side of eq 26 contributes to the reaction probability. Even in this case, however, both terms in the diabatic analogue of eq 11 may play a role, because adiabatic and diabatic surfaces need not coincide asymptotically.[12,13] This is just the case for H + H_2 to be presented below.

III. Computational Details

In this section we describe the calculation of reaction probabilities by the scheme developed above. In the following we proceed with the coupled surface calculations; the uncoupled surface calculations trivially follow from them. The time-dependent Schrödinger equation (TDSE) is solved numerically in the diabatic electronic representation on a grid in the (R,r,γ) space using the matrix Hamiltonian in eq 1. For an explicitly time-independent Hamiltonian the solution reads

$$\Psi^d(R,r,\gamma,t) = \exp\left[\frac{-iH^d t}{\hbar}\right]\Psi^d(R,r,\gamma,0) \quad (27)$$

Here $\Psi^d(R,r,\gamma,0)$ is the initial wave function pertinent to the

reactants in the diabatic electronic representation and $\Psi^{d}(R,r,\gamma,t)$ is the wave function at time t.

In a reactive scattering study the initial wave function is prepared in the asymptotic reactant channel where the interaction potential almost vanishes. In such a situation the initial wave function pertinent to the H + H_2 reacting system can be written as a product of the translational wave function $F(R)$ for the motion along R and the rovibrational wave function $\Phi_{vj}(r)$ of the H_2 molecule. We locate the wave function initially on the repulsive lower adiabatic sheet (V_-) of the DMBE PES. In the present case for, $J = 0$, it is given by

$$\Psi^{ad}(R,r,\gamma,0) = F(R)\Phi_{vj}(r)\sqrt{\frac{2j+1}{2}}P_j(\cos\gamma)\begin{pmatrix}1\\0\end{pmatrix} \quad (28)$$

We choose a minimum uncertainty Gaussian wave packet (GWP) for $F(R)$:

$$F(R) = \left(\frac{1}{2\pi\delta^2}\right)^{1/4}\exp\left[-\frac{(R-R_0)^2}{4\delta^2} - ik_0(R-R_0)\right] \quad (29)$$

The quantity δ is the width parameter of the GWP, and R_0 and k_0 correspond to the location of its maximum in the coordinate and momentum space, respectively. The functions $\Phi_{vj}(r)$ along with the normalized Legendre polynomials ($P_j(\cos\gamma)$) represents the rovibrational eigenfunction corresponding to a (v,j) state of the H_2 molecule. The function $\Phi_{vj}(r)$ are obtained by solving the eigenvalue equation of the free H_2 molecule:

$$\left[-\frac{\hbar^2}{2\mu'}\frac{d^2}{dr'^2} + V(r') + \frac{j(j+1)\hbar^2}{2\mu' r'^2}\right]\Phi_{vj}(r') = \epsilon_{vj}\Phi_{vj}(r') \quad (30)$$

Here μ' is the reduced mass of the H_2 molecule, ϵ_{vj} the energy eigenvalue, $r' = r\,(\mu/\mu')^{1/2}$ the unscaled internuclear distance, and $V(r')$ is the potential energy of the H_2 molecule obtained from the DMBE PES by setting $R \rightarrow \infty$. We used the sine-DVR approach of Colbert and Miller[43] to solve the above eigenvalue equation.

The initial wave function defined in eq 28 is transformed to the diabatic representation by using the $\boldsymbol{S}$ matrix (eq 4) prior to its propagation. In the diabatic representation the initial wave function can be written in the vector notation as

$$\Psi^{d}(R,r,\gamma,0) = \psi_1{}^{d}(R,r,\gamma,0)\begin{pmatrix}1\\0\end{pmatrix} + \psi_2{}^{d}(R,r,\gamma,0)\begin{pmatrix}0\\1\end{pmatrix} \quad (31)$$

where $\binom{1}{0}$ and $\binom{0}{1}$ indicate the first and the second diabatic electronic state with energy U_{11} and U_{22}, respectively. Note that these are different from the one introduced in eq 28. $\psi_1{}^{d}$ and $\psi_2{}^{d}$ are the nuclear wave functions in the respective electronic states depending on the set of Jacobi coordinates. To follow the nuclear dynamics the TDSE (eq 27) is solved with the above initial diabatic wave function. The exponential time evolution operator in eq 27 is evaluated by dividing the time axis into N segments of length Δt. The exponential operator at each time step is then approximated by the split-operator method,[44]

$$\exp\left[\frac{-iH^{d}\Delta t}{\hbar}\right] = \exp\left[\frac{-iH^{el}\Delta t}{2\hbar}\right]\exp\left[\frac{-i\mathbf{j}^2\Delta t}{4I\hbar}\mathbf{1}\right]\times \exp\left[\frac{-iT(R,r)\Delta t}{\hbar}\mathbf{1}\right]\left[\frac{-i\mathbf{j}^2\Delta t}{4I\hbar}\mathbf{1}\right]\exp\left[\frac{-iH^{el}\Delta t}{2\hbar}\right] + O[(\Delta t)^3] \quad (32)$$

where $T(R,r) = (P_R{}^2 + P_r{}^2)/2\mu$ is the total radial kinetic energy operator. $\mathbf{1}$ represents the 2 × 2 unit matrix. The electronic Hamiltonian H^{el} can be decomposed into

$$H^{el} = \begin{pmatrix}U_{11} & 0\\0 & U_{22}\end{pmatrix} + U_{12}\begin{pmatrix}0 & 1\\1 & 0\end{pmatrix} \quad (33)$$

Since the diagonal and the off-diagonal parts of H^{el} do not commute with each other, the propagator containing it in eq 32 is further written as

$$e^{-iH^{el}\Delta t/2\hbar} = e^{-i\begin{pmatrix}U_{11} & 0\\0 & U_{22}\end{pmatrix}\Delta t/4\hbar}e^{-iU_{12}\begin{pmatrix}0 & 1\\1 & 0\end{pmatrix}\Delta t/2\hbar}e^{-i\begin{pmatrix}U_{11} & 0\\0 & U_{22}\end{pmatrix}\Delta t/4\hbar} \quad (34)$$

The exponent containing the off-diagonal matrix elements is now expressed in terms of the 2 × 2 Pauli matrix

$$e^{-iU_{12}\begin{pmatrix}0 & 1\\1 & 0\end{pmatrix}\Delta t/2\hbar} = \begin{pmatrix}\cos(U_{12}\Delta t/2\hbar) & -i\sin(U_{12}\Delta t/2\hbar)\\ -i\sin(U_{12}\Delta t/2\hbar) & \cos(U_{12}\Delta t/2\hbar)\end{pmatrix} \quad (35)$$

Equation 32 is used in conjunction with the fast Fourier transform method[45] to evaluate the action of the exponential containing the radial kinetic energy operator and the discrete variable representation method[46] to evaluate the exponential containing the rotational kinetic energy operator ($\mathbf{j}^2/2I$) on the wave function. The coordinate grid consists of equally spaced points R_l and r_m along the Jacobi distances R and r, respectively. The grid along the Jacobi angle γ is chosen as the nodes of a n-point Gauss−Legendre quadrature (GLQ).[47] The initial adiabatic wave function at each node (R_l,r_m,γ_n) of this grid is given by

$$\Psi^{ad}(R_l,r_m,\gamma_n,0) = \sqrt{w_n}F(R_l)\Phi_{vj}(r_m)\sqrt{\frac{2j+1}{2}}P_j(\cos\gamma_n)\begin{pmatrix}1\\0\end{pmatrix} \quad (36)$$

where w_n is the weight of the GLQ associated with the grid point n.

In dynamical studies involving scattering systems, as the WP moves forward in time, its fast moving components approach the grid boundaries and are no longer relevant for the rest of the dynamics.[29] Therefore, to avoid unphysical reflections or wrap arounds of these components from the boundaries of a finite sized grid, the WP at each time step is multiplied by a damping function[48]

$$f(X_i) = \sin\left[\frac{\pi(X_{mask} + \Delta X_{mask} - X_i)}{2\,\Delta X_{mask}}\right] \qquad X_i \geq X_{mask} \quad (37)$$

which is activated outside the dividing line ($r_d > 0$) in the product channel and also in the asymptotic reactant channel. X_{mask} is the point at which the damping function is initiated, and ΔX_{mask} ($=X_{max} - X_{mask}$) is the width of X over which the function decays from 1 to 0, with X_{max} being the maximum value of X in that direction, in a particular channel. The properties of the initial WP and the grid parameters used for the numerical calculations are listed in Table 1.

The time dependence of the adiabatic electronic populations can be calculated either by using the $\boldsymbol{S}$ matrix (eq 4) or by defining suitable adiabatic projection operators. The $\boldsymbol{S}$ matrix is a double-valued function of the coordinates and possesses a branch point at the conical intersection. This problem is circumvented by using adiabatic projectors in the diabatic

TABLE 1: Numerical Grid Parameters and Properties of the Initial Wave function Used in the Calculations of Reaction Probabilities

param	value	description
$N_R/N_r/N_\gamma$	128/64/48	no. of grid points
R_{min}/R_{max} (a_0)	0.10/15.34	extension of the grid along R
r_{min}/r_{max} (a_0)	0.50/8.06	extension of the grid along r
$\Delta R = \Delta r$ (a_0)	0.12	grid spacings along R and r
r_I (a_0)	4.1	location of the dividing surface in the product channel
R_{mask}/r_{mask} (a_0)	11.74/4.70	starting point of the masking function
R_0 (a_0)	10.5	initial location of the center of the GWP in the coordinate space
κ_0 (au)	12.48	initial location of the center of the GWP in the momentum space
δ (a_0)	0.16	initial width param of the GWP
Δt (fs)	0.1347	length of the time step used in the WP propagation
T (fs)	413.76	tot. propagation time

electronic representation[2,49]

$$P_-^{ad} = \boldsymbol{S}\begin{pmatrix}1 & 0\\ 0 & 0\end{pmatrix}\boldsymbol{S}^\dagger = \frac{1}{2} - \frac{1}{2(\Delta^2 + U_{12}^2)^{1/2}}\begin{pmatrix}-\Delta & U_{12}\\ U_{12} & \Delta\end{pmatrix}$$

$$P_+^{ad} = 1 - P_-^{ad} \tag{38}$$

where $\mp$ refers to the lower and the upper adiabatic sheet, respectively. Δ is half of the energy gap between the two diabatic surfaces. The expectation values of the above projectors define the electronic populations in the respective electronic states.

IV. Results and Discussion

In this section we apply the general formalism of section II to calculate the initial state-specific and energy resolved reaction probabilities of (R1). The reaction probabilities are calculated across a dividing surface located at $r_d = 4.1a_0$ at an energy interval of 9×10^{-3} eV. The convergence of the results is checked with respect to the numerical grid parameters given in Table 1.

The total reaction probability (summed over all open vibrational (v') and rotational (j') states of the product H_2 at a given energy) of (R1), for reactant H_2 ($v = 0, j = 0$) as a function of the total energy E is plotted in Figure 1. The coupled-surface results are shown by the solid line. The uncoupled (lower adiabatic) surface results without and with the diagonal correction are shown by the short- and long-dashed lines, respectively. The initial WP is prepared on the lower adiabatic sheet as is the case in all previous studies of this system. The energy distribution of the initial translational GWP is shown in the inset. It can be seen that the translational components of the initial WP cover a broad range of energies from the onset of the reaction threshold at $E = 0.55$ eV to the three-body dissociation limit at $E = 4.74$ eV. Therefore, the reaction probabilities in that range of energies can be reliably obtained with this WP. The coupled-surface results are obtained by analyzing the reactive flux in the adiabatic picture through eq 26. We find that only the first term of eq 26 contributes to the reaction probability, which is further discussed below. The resonance structures and their energetic locations are same in the coupled and uncoupled surface results. The difference between the coupled and uncoupled surface (without the diagonal correction) results is 2−3% at low energies. At high energies this difference

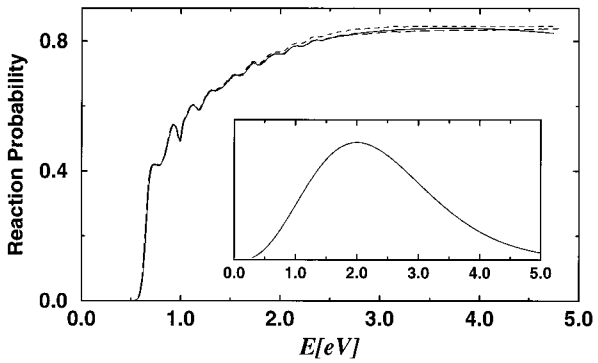

Figure 1. Total reaction probability as a function of the total energy E (H, H_2 translational + H_2 rovibrational) for the $H + H_2(v = 0, j = 0) \rightarrow H_2(\Sigma v', \Sigma j') + H$ exchange reaction on the DMBE PES in three-dimensions and for total angular momentum $J = 0$. The energy E is measured from the minimum of the H_2 potential. The coupled-surface results (obtained by analyzing the reactive flux in the adiabatic electronic picture, eq 26) are shown by the solid line. The uncoupled surface results with and without the diagonal BH correction are shown by the long- and short-dashed lines, respectively. The energy distribution of the initial translational GWP is shown in the inset.

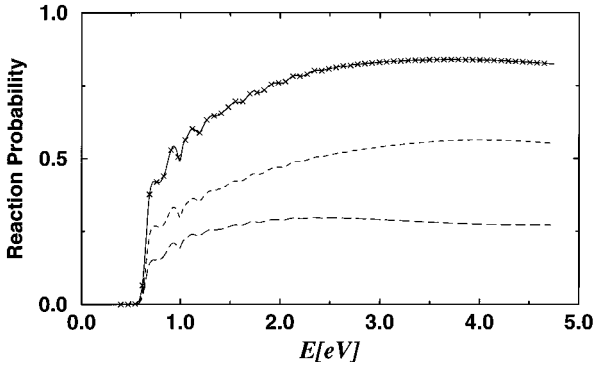

Figure 2. Same as in Figure 1, obtained by analyzing the reactive flux in the diabatic electronic picture, eq 11. The reaction probability curves obtained on the diabatic electronic states U_{11} and U_{22} are shown by the short- and long-dashed lines, respectively. The sum of the two diabatic probabilities is superimposed on the adiabatic coupled-surface results (solid line) of Figure 1 on a coarse energy grid and is indicated by crosses.

increases only slightly. The minimum of the seam of conical intersections of H_3 occurs at ~2.74 eV.[16] Therefore, the coupled-surface results are expected to differ more from the uncoupled ones beyond this energy. However, it can be seen from Figure 1 that the impact of the conical intersection on the $H_2(v = 0, j = 0)$ reaction probabilities is negligibly small. The small deviations become even smaller when including the diagonal correction.

The same reaction probability calculated in the diabatic electronic picture through eq 11 is shown in Figure 2. The probability values shown by the short- and long-dashed lines are obtained by analyzing the reactive flux on the two component diabatic electronic states U_{11} and U_{22}, respectively (represented by the first and the second term of eq 11). The sum of these two components is indicated by the crosses and is superimposed on the coupled surface results (solid line) of Figure 1, obtained in the adiabatic electronic picture from the first term of eq 26. For clarity of presentation we show the crosses on a coarse grid of energy values. It is clear from Figure 2 that the second and the third terms of eq 26 do not contribute to the reaction probability of $H + H_2(v = 0, j = 0)$ in the energy range of the present investigations. This is because on the upper adiabatic surface product H_2 is asymptotically prepared in its

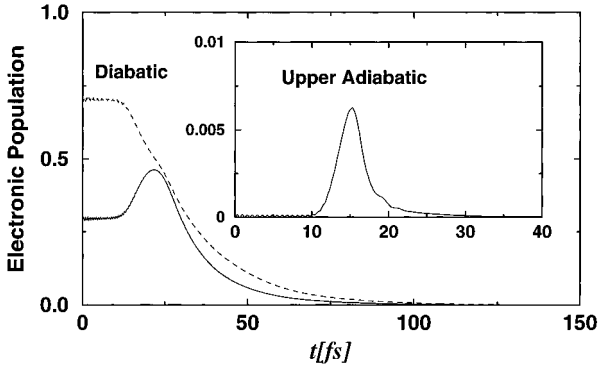

Figure 3. Electronic population dynamics for the H + $H_2(v = 0, j = 0) \rightarrow H_2(\Sigma v', \Sigma j') + H$ exchange reaction. The populations of the two component diabatic electronic states U_{11} and U_{22} are shown by the dashed and solid lines, respectively. Because of the damping function activated at the grid edge, the above populations approach to zero at longer times. The population of the upper adiabatic electronic state (V_+) is shown in the inset.

$^3\Sigma_u$ state which has its minimum at $E \sim 4.74$ eV,[16] at the onset of the three-body dissociation. Therefore, in the present investigations this channel remains energetically closed and does not contribute to the reaction probability. This is numerically checked further from the reaction probabilities obtained from the second term of eq 26. They are all zero until the fourth decimal place which shows that the second and the third terms are zero individually, not just their sum. Despite a difference in the magnitude of the reaction probabilities, the two component diabatic probability curves exhibit similar resonance structures.

To better understand the similarity between the coupled and the uncoupled surface results we show the time evolution of the electronic populations in Figure 3. The initial WP corresponds to $H_2(v = 0, j = 0)$ and is again prepared in the asymptotic reactant channel of the lower adiabatic sheet. (It is transformed to the diabatic representation using the ***S*** matrix of eq 4 prior to propagation). As can be seen from Figure 3, we obtain a 0.71/0.29 population of the two component diabatic electronic states (shown by the dashed and solid lines) at $t = 0$. Therefore, the diabatic potentials do not approach the asymptotic adiabatic states of H + H_2 but represent a mixture of them. A similar kind of behavior of the diabatic electronic states has been found, e.g., for the ozone[12] and hydrogen disulfide molecules.[13] This may be a surprising feature of the diabatization procedure but, in practice, is often unavoidable. However, since the adiabatic states are well separated asymptotically, preparing an initial WP on the adiabatic electronic state and propagating it in the diabatic electronic representation and finally transforming it back to the adiabatic states before analysis is expected to have only little relevance of this "artifact" on the dynamics. The coincidence of the reaction probabilities obtained in the diabatic and the adiabatic picture (see Figure 2) also adds an evidence to this remark. The population of the upper adiabatic electronic state is shown in the inset of Figure 3. The population of this state reaches a maximum value of $\sim 6.25 \times 10^{-3}$ after $\sim$15 fs. Therefore, only $\sim$0.625% of the WP traverses to the upper adiabatic cone during the course of the entire dynamics. This can hardly have any major impact on the dynamics. The minimum energy path for the H + H_2 reactive scattering process occurs at the collinear arrangement of the three nuclei which is far away from the seam of conical intersections, occurring at the D_{3h} arrangements of the three nuclei. The classical barrier height of the collinear saddle point on the lower adiabatic sheet is $\sim$0.42 eV, whereas the minimum of the seam of conical intersections occurs at $\sim$2.74 eV at the equilateral triangular

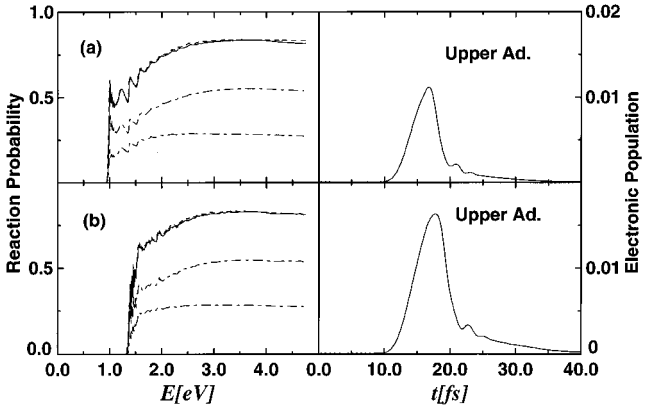

Figure 4. Same as in Figure 1, for H + $H_2(v, j = 0) \rightarrow H_2(\Sigma v', \Sigma j')$ + H reaction. Reaction probabilities for $v = 1$ and $v = 2$ are shown in panels a and b, respectively. The solid and the dashed lines in each panel indicate the adiabatic coupled-surface and uncoupled- (without the diagonal correction) surface results, respectively. The results obtained in the diabatic electronic picture are shown by the dot−dashed lines in each panel. In the right-hand side of each panel the corresponding electronic population of the upper adiabatic electronic state is shown as a function of the propagation time.

geometry.[16] Apparently also for higher energies a major part of the reactive flux is directed via the low-energy transition state conformation. A similar numerical observation has been made earlier in a bound-state calculation of electronically excited states of SO_2.[50]

In Figure 4 we show the reaction probabilities obtained with the vibrationally excited reactant (a) $H_2(v = 1, j = 0)$ and (b) $H_2(v = 2, j = 0)$. The coupled and the uncoupled (without the diagonal correction) surface results are shown in each panel by the full and the dashed lines, respectively. The coupled-surface results are obtained by analyzing the reactive flux in the adiabatic electronic picture. The probability curves obtained by using the diabatic electronic basis are also included in the figures and are shown by the dot−dashed lines. Again, the sum of the reaction probabilities obtained in the diabatic picture equals those obtained in the adiabatic picture. For the coupled surface results of the adiabatic picture only contributions from the first term of eq 26 are shown; the contributions from the second and third terms are found to be almost zero. In the right-hand side of each panel the corresponding electronic populations of the upper adiabatic sheet are plotted as a function of the propagation time. As in case of $H_2(v = 0, j = 0)$, the difference between the coupled and the uncoupled-surface results for vibrationally excited H_2 is very small. The resonance structures and their energetic locations are also the same in the coupled and the uncoupled surface results. A closer inspection of the electronic populations in Figure 4 reveals that for vibrationally excited H_2 a larger fraction of the WP traverses to the upper adiabatic sheet during the reaction. For instance, $\sim$1% and $\sim$1.6% of the WP traverse to the upper cone during the reaction for $v = 1$ and $v = 2$, respectively. Also, the population maximum occurs at a slightly later propagation time on vibrational excitation.

To assess the accuracy of the DMBE PES, which relies on the analytic continuation approach for the upper adiabatic sheet, additional ab initio calculations were performed. They aim to globally represent both the adiabatic sheets of the ground electronic manifold of H_3 and the associated nonadiabatic coupling elements between them. These calculations are similar to those reported by Varandas et al.[16] in their extension of the Liu−Siegbahn[19] full configuration interaction (CI) treatment of H_3. The adiabatic wave functions and derivative couplings were

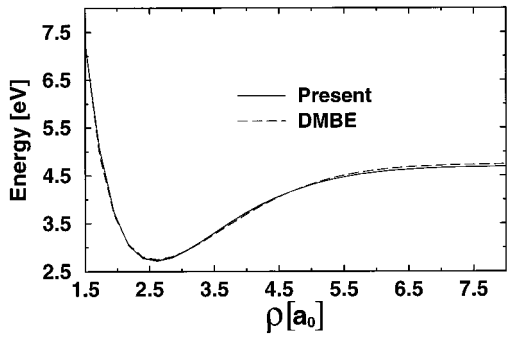

Figure 5. Cuts of the adiabatic potential energy surfaces of H_3 as a function of the hyperradius ρ for $\theta = 0.1°$ and $\phi = 20°$ (nearly along the seam of conical intersections occurring at $\theta = 0°$). The two adiabatic potential energy surfaces $V_{\mp}$ are degenerate for this geometry. The new ab initio results are shown by the solid line, and the potential energies from the DMBE PES for the same geometry are indicated by the dashed line. The minimum in the potential energy curve represents the minimum of the seam of conical intersections occurring at 2.74 eV for $\rho = 2.5a_0$ in both cases.

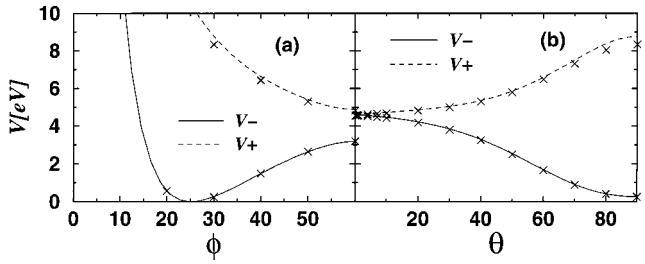

Figure 6. Cuts of the adiabatic potential energy surfaces of H_3 (a) along ϕ (in degrees) for $\rho = 6.0a_0$ and $\theta = 90°$ and (b) along θ (in degrees) for $\rho = 6.0a_0$ and $\phi = 30°$. $\theta = 90°$ corresponds to the collinear arrangement of the three nuclei. The solid and dashed lines in each panel represent the potential energy values V_- and V_+, respectively, from the DMBE PES. The new ab initio results are superimposed on them and are indicated by the crosses.

determined from second-order CI[51] wave functions based on a three electron, three orbital, active space. The molecular orbitals were determined from a complete active space[52] state-average multiconfigurational self-consistent field procedure in which two $2A'$ states were averaged with weights (0.505,0.495) based on (6s3p1d) contracted Gaussian basis sets on the hydrogen. We show only a few cuts of these new potential energy surfaces for some relevant geometries of H_3 which fit to the need of the present purposes and compare them with similar cuts from the DMBE PES. The full presentation of our new potential energy surfaces and dynamical studies on them is beyond the scope of the present paper and will be considered in a future publication. In what follows we will use the principal axes of inertia symmetrized hyperspherical coordinates (ρ,ϕ,θ) of Kuppermann (see eqs 148−153 and164 in ref 53) in discussing the properties of the potential energy surfaces. In this coordinate system, $\theta = 0°$ corresponds to the equilateral triangular configuration and $\theta = 90°$ corresponds to the collinear configuration. This choice is made because in our future dynamical studies we wish to explore the advantage of using the hyperspherical coordinates for a symmetric triatomic system.

In Figure 5 we plot the potential energy surfaces along the hyperradius ρ for fixed values of $\theta = 0.1°$ and $\phi = 20°$. The finite value of θ has been chosen for technical reasons. It is small enough that (irrespective of ϕ) the cuts of Figure 5 represents the D_{3h} conformations, with ρ being $3^{1/4}$ (for H_3) times the side length of the equilateral triangle. Note that $V_- = V_+$ for these (and only these) geometries so that Figure 5 represent the potential energies along the seam of conical intersections. The close similarity between the new ab initio results (full line) and the DMBE surface (dashed line) is satisfying but not quite unexpected because the analytic continuation technique should be accurate near D_{3h} geometries.

More significant are comparisons for non-D_{3h} conformations as underlying Figure 6. In panel a we report results along ϕ for $\theta = 90°$ (collinear arrangement of nuclei), and in panel b are results for $\theta = 0°$ (D_{3h}) − 90° (collinear) for $\phi = 30°$. Despite the large energetic splitting between V_+ and V_- the agreement between the new ab initio data and the DMBE surface[16] is remarkably good. We take this as an indication that the DMBE surface is accurate enough so that at least the comparison between coupled-surface and uncoupled-surface results of Figures 1−4 should not be seriously affected. A numerical test of the accuracy of the diabatization scheme adopted is certainly also desirable and, in fact, planned by us for the near future. It is, however, beyond the scope of the present article.

V. Summary and Outlook

The reactive scattering dynamics of bimolecular collision processes occurring on a single PES is well studied in the literature. In contrast to that, only in recent years effort is made to understand the implications of nonadiabatic interactions in a reactive scattering process. We have presented here a concise description of the initial state-specific reactive scattering dynamics on coupled electronic potential energy surfaces. We focused on a ($E \times \epsilon$)-JT conical intersection and a time-dependent wave packet method as regards the nuclear dynamics. Particularly we described the analysis of the reactive flux of the WP in order to calculate the initial state-specific and energy resolved total reaction probability. The initial WP is prepared on an adiabatic electronic state and is propagated in a suitable diabatic electronic representation. One needs to resort to the latter representation in order to avoid the diverging (at the seam of intersections of the potential energy surfaces) nonadiabatic coupling elements appearing in the adiabatic electronic basis. The final analysis of the reactive flux is carried out both in the adiabatic and in the diabatic electronic representations. While the representation of the flux operator is diagonal in the diabatic electronic basis, it contains off-diagonal elements (arising from the off-diagonal kinetic coupling elements) in the adiabatic electronic basis.

The above formalism is applied to calculate the state-specific and energy resolved total reaction probabilities of the $H + H_2$ exchange reaction on the DMBE PES. The reaction probabilities obtained in the coupled-surface calculations differ only slightly from those obtained from the single surface calculations. The coupled-surface results at high energies can essentially be reproduced by the single surface calculation including the diagonal correction to the BO Hamiltonian. Especially, all resonance structures and their energetic locations are found to be similar in both the coupled- and uncoupled-surface results. The sum of the reaction probabilities obtained in the diabatic representation (eq 11) equals that obtained in the adiabatic picture considering only the first term of eq 26. On the upper adiabatic sheet, H_2 is produced in its $^3\Sigma_u$ state and the energetic minimum of this state occurs at the onset of the three-body dissociation (~4.74 eV). Therefore, in the energy range of the present investigations the last two terms of eq 26 do not contribute to the reaction probability. The resonance structures and their energetic locations are found to be similar in both the coupled and uncoupled surface results.

The minimum energy path for the reactive scattering processes in $H + H_2$ occurs at the collinear arrangement of the

three nuclei, which is far away from the seam of conical intersections occurring at the D_{3h} configuration. Beyond the minimum of the seam of conical intersections occurring at ~2.74 eV, the noncollinear collisions might be expected to make significant contributions in the reactive scattering dynamics. However, the region of the space covered by the configuration of the three nuclei for which the two surfaces are nearly degenerate is very small and any slight deviation form these configurations leads to a significant energy splitting of the two surfaces. We find only a very small fraction the WP (less than 2%) traversing the upper adiabatic cone during the course of the reaction. Therefore, no dramatic effects of the conical intersections on the reaction probability are unveiled by the present investigations.

To assess the accuracy of the DMBE PES, we refer to new ab initio calculations which have been carried out to globally represent the two adiabatic sheet of the ground electronic manifold of H_3 and the associated nonadiabatic couplings between them.[54] We find these new data compare quite well to the DMBE PES. This confirms the accuracy of the DMBE PES. The presentation of the full surfaces and the dynamical results based on them and on the ensuing nonadiabatic couplings will be considered in a future publication.

Acknowledgment. This study is supported in part by a grant from the Deutsche Forschungsgemeinschaft. S.M. gratefully acknowledges a research grant from the Department of Science and Technology, New Delhi, under the young scientists scheme. We thank David R. Yarkony for providing us with the new ab initio results and a careful reading of the manuscript. We also thank Hans-Dieter Meyer for his interest in this work and a careful reading of the manuscript.

References and Notes

(1) Teller, E. *J. Phys. Chem*. **1937**, *41*, 109. Herzberg, G.; Longuet-Higgins, H. C. *Discuss. Faraday Soc*. **1963**, *35*, 77. Carrington, T. *Discuss. Faraday Soc*. **1972**, *53*, 27; *Acc. Chem. Res*. **1974**, *7*, 20. Davidson, E. R. *J. Am. Chem. Soc*. **1977**, *99*, 397.

(2) Köppel, H.; Domcke, W.; Cederbaum, L. S. *Adv. Chem. Phys.* **1984**, *57*, 59.

(3) Bernardi, F.; Olivucci, M.; Robb, M. *Chem. Soc. Rev.* **1996**, *25*, 321.

(4) Domcke, W.; Stock, G. *Adv. Chem. Phys*. **1997**, *100*, 1.

(5) Yarkony, D. R. *Acc. Chem. Res*. **1998**, *31*, 511.

(6) Köppel, H.; Domcke, W. In *Encyclopedia of Computational Chemistry*; Schleyer, P. v. R., Ed.; Wiley: New York, 1998.

(7) *Chem. Phys.* **2000**, *259*, 121−337 (special issue on conical intersections).

(8) Baer, R.; Charutz, D. M.; Kosloff, R.; Baer, M. *J. Chem. Phys*. **1996**, *105*, 9141.

(9) Drukker, K.; Schatz, G. C. *J. Chem. Phys*. **1999**, *111*, 2451.

(10) Hsu, Y.-T.; Liu, K.; Pederson, L. A.; Schatz, G. C. *J. Chem. Phys*. **1999**, *111*, 7931.

(11) Whiteley, T. W.; Dobbyn, A. J.; Connor, J. N. L.; Schatz, G. C. *Phys. Chem. Chem. Phys*. **2000**, *2*, 549.

(12) Flöthmann, H.; et al. *J. Chem. Phys*. **1997**, *107*, 7296.

(13) Simah, D.; Hartke, B.; Werner, H.-J. *J. Chem. Phys*. **1999**, *111*, 4523.

(14) Yarkony, D. R. *J. Chem. Phys*., in press.

(15) Lichten, W. *Phys. Rev.* **1963**, *131*, 229; **1967**, *164*, 131. Smith, F. T. *Phys. Rev*. **1969**, *179*, 111. O'Malley, T. F. *Adv. At. Mol. Phys*. **1971**, *7*, 223. For an overview of more recent work see, for example: Pacher, T.; Cederbaum, L. S.; Köppel, H. *Adv. Chem. Phys*. **1993**, *84*, 293.

(16) Varandas, A. J. C.; Brown, F. B.; Mead, C. A.; Truhlar, D. G.; Blais, N. C. *J. Chem. Phys.* **1987**, *86*, 6258.

(17) Porter, R. N.; Stevens, R. M.; Karplus, M. *J. Chem. Phys*. **1968**, *49*, 5163.

(18) Englman, R. *The Jahn−Teller Effect in Molecules and Crystals*; Wiley-Interscience: New York, 1972.

(19) Siegbahn, P.; Liu, B. *J. Chem. Phys*. **1978**, *68*, 2466. Truhlar, D. G.; Horowitz, C. J. *J. Chem. Phys*. **1978**, *68*, 2466.

(20) Boothroyd, A. I.; Keogh, W. J.; Martin, P. G.; Peterson, M. R. *J. Chem. Phys*. **1996**, *104*, 7139.

(21) Wu, Y.-S. M.; Kuppermann, A.; Lepetit, B. *Chem. Phys. Lett*. **1991**, 319. Wu, Y.-S. M.; Kuppermann, A. *Chem. Phys. Lett*. **1993**, *201*, 178. Kuppermann, A.; Wu, Y.-S. M. *Chem. Phys. Lett*. **1993**, *205*, 577.

(22) Wu, Y.-S. M.; Kuppermann, A. *Chem. Phys. Lett*. **1995**, *235*, 105. Kuppermann, A.; Wu, Y.-S. M. *Chem. Phys. Lett*. **1995**, *241*, 229.

(23) Schnieder, L.; Seekamp-Rahn, K.; Borkowski, J.; Wrede, E.; Welge, K.; Aoiz, F. J.; Bañares, L.; D'Mello, M. J.; Herrero, V. J.; Sáez Rábanos, V.; Wyatt, R. E. *Science* **1995**, *269*, 207. Wrede, E.; Schnieder, L.; Welge, K. H.; Aoiz, F. J.; Bañares, L.; Castillo, J. F.; Martínez-Haya, B.; Herrero, V. J. *J. Chem. Phys.* **1999**, *110*, 9971.

(24) Kendrick, B. K. *J. Chem. Phys*. **2000**, *112*, 5679.

(25) Varandas, A. J. C.; Yu, H. G. *J. Chem. Soc., Faraday Trans*. **1997**, *93*, 819.

(26) Varandas, A. J. C.; Yu, H. G. *Chem. Phys. Lett*. **1996**, *259*, 336.

(27) Bruckmeier, R.; Wunderlich, Ch.; Figger, H. *Phys. Rev. Lett*. **1994**, *72*, 2250.

(28) Mahapatra, S.; Köppel, H. *J. Chem. Phys*. **1998**, *109*, 1721; *Phys. Rev. Lett*. **1998**, *81*, 3116; *Faraday Discuss*. **1998**, *110*, 248.

(29) Neuhauser, D.; Baer, M. *J. Chem. Phys*. **1989**, *91*, 4651. Neuhauser, D.; Baer, M.; Judson, R. S.; Kouri, D. J. *J. Chem. Phys*. **1990**, 93, 312; *Chem. Phys. Lett*. **1990**, *169*, 372.

(30) Zhang, D. H.; Zhang, J. Z. H. *J. Chem. Phys.* **1993**, *99*, 5615; **1994**, *100*, 2697; 5631; **1994**, *101*, 1146; 3671.

(31) Manthe, U. *Chem. Phys. Lett*. **1995**, *241*, 497.

(32) Balakrishnan, N.; Kalyanaraman, C.; Sathyamurthy, N. *Phys. Rep*. **1997**, *280*, 79. Beck, M.; Jäckle, A.; Worth, G. A.; Meyer, H.-D. *Phys. Rep*. **2000**, *324*, 1. Nyman, G.; Yu, H.-G. *Rep. Prog. Phys*. **2000**, *63*, 1001.

(33) Mahapatra, S.; Sathyamurthy, N. *J. Chem. Phys*. **1997**, *107*, 6621. Mahapatra, S. *Phys. Chem. Chem. Phys.* **2000**, *2*, 671.

(34) Tennyson, J.; Sutcliffe, B. T. *J. Chem. Phys*. **1982**, *77*, 4061.

(35) Köppel, H.; Mahapatra, S.; Thiel, A. In *Proceedings of the XIV International Symposium on Electron−Phonon Dynamics and Jahn−Teller Effect*; Bevilacqua, G., Martinelli, L., Terzi, N., Eds.; World Scientific: Singapore, 1999; pp 327−334.

(36) Thiel, A.; Köppel, H. *J. Chem. Phys*. **1999**, *110*, 9371.

(37) Yarkony, D. R. *J. Chem. Phys*. **2000**, *112*, 2111.

(38) Miller, W. H. *J. Phys. Chem*. **1998**, *102*, 793 and references therein.

(39) Park, T. J.; Light, J. C. *J. Chem. Phys*. **1988**, *88*, 4897.

(40) Born, M.; Huang, K. *Dynamical Theory of Crystal Lattices*; Oxford University Press: New York, 1954.

(41) Schön, J.; Köppel, H. *J. Chem. Phys*. **1995**, *103*, 9292.

(42) Kutzelnigg, W. *Mol. Phys*. **1997**, *90*, 909.

(43) Colbert, D. T.; Miller, W. H. *J. Chem. Phys*. **1992**, *96*, 1982.

(44) Feit, M. D.; Fleck, J. A., Jr.; Steiger, A. *J. Comput. Phys.* **1982**, *47*, 412.

(45) Kosloff, D.; Kosloff, R. *J. Comput. Phys*. **1983**, *52*, 35.

(46) Bačić, Z.; Light, J. C. *Annu. Rev. Phys. Chem*. **1989**, *40*, 469. Quéré, F.; Leforestier, C. *J. Chem. Phys.* **1990**, *92*, 247. Corey, G. C.; Lemoine, D. *J. Chem. Phys*. **1992**, *97*, 4115.

(47) Press, W. H.; Flannery, B. P.; Teukolsky, S. A.; Vetterling, W. T. *Numerical Recipes: The Art of Scientific Computing*; Cambridge University Press: Cambridge, U.K., 1986; p 125.

(48) Mahapatra, S.; Sathyamurthy, N. *J. Chem. Soc., Faraday Trans*. **1997**, *93*, 773.

(49) Manthe, U.; Köppel, H. *J. Chem. Phys*. **1990**, *93*, 345, 1658.

(50) Müller, H.; Köppel, H. *Chem. Phys*. **1994**, *183*, 107.

(51) Silverstone, H. J.; Sinanoglu, O. *J. Chem. Phys.* **1996**, *44*, 1899.

(52) Roos, B. O. *Int. J. Quantum Chem. Symp*. **1980**, *14*, 175. Roos, B. O.; Taylor, P. R.; Siegbahn, P. E. M. *Chem. Phys*. **1980**, *48*, 157. Siegbahn, P.; Heiberg, A.; Roos, B.; Levy, B. *Phys. Scr*. **1980**, *21*, 323.

(53) Kuppermann, A. In *Dynamics of Molecules and Chemical Reactions*; Wyatt, R. E., Zhang, J. Z. H., Eds.; Marcel Dekker: New York, 1996.

(54) Mahapatra, S.; Köppel, H.; Cederbaum, L. S.; Yarkony, D. R. To be published.